

Densities, temperatures, pressures, and abundances derived from O II recombination lines in H II regions and their implications

Antonio Peimbert¹

antonio@astro.unam.mx

and

Manuel Peimbert¹

peimbert@astro.unam.mx

ABSTRACT

Based on high quality observations of multiplet V1 of O II and the NLTE atomic computations of O II we study the density and temperature of a sample of H II regions. We find that the signature for oxygen rich clumps of high density and low temperature is absent in all objects of our sample: one extragalactic and eight Galactic H II regions. The temperatures derived from: a) recombination lines of O II, and b) recombination lines of H I together with Balmer continua are lower than those derived from forbidden lines, while the densities derived from recombination lines of O II are similar or smaller than densities derived from forbidden lines. Electron pressures derived from collisionally excited lines are about two times larger than those derived from recombination lines. These results imply that the proper abundances are those derived from recombination lines and suggest that other processes in addition to direct photoionization, such as dissipation of turbulent energy in shocks, magnetic reconnection, and shadowed regions, might be responsible for the large ADF and t^2 values observed in H II regions.

Subject headings: galaxies: abundances — galaxies: ISM — H II regions— ISM: abundances

¹Instituto de Astronomía, Universidad Nacional Autónoma de México, Apdo. Postal 70-264, México 04510 D.F., Mexico

1. Introduction

Since the collisional intensities of O lines, as well as other heavy elements, are several orders of magnitude stronger than the recombination lines, most abundances of heavy elements relative to those of hydrogen have been derived from collisionally excited lines. In addition usually collisional abundances are only derived under the assumption of chemical homogeneity and constant temperature.

O/H abundance ratios derived from recombination lines of O and H are higher than those derived from the ratio of a collisionally excited line (CL) of oxygen to a recombination line (RL) of H, this effect is called the abundance discrepancy problem, and the ratio of both types of abundances is called the abundance discrepancy factor (ADF). This problem also applies to other heavy elements like C, N, and Ne.

There are several explanations for the ADFs present in the literature for example: temperature variations in a homogeneous medium, inhomogeneous chemical composition, errors in the atomic parameters, and overestimation of the intensity of weak recombination lines. Errors in the atomic parameters have been ruled out because the ADF values vary from object to object, and the overestimation of the intensity of the weak lines has also been ruled out because the ADF problem persists for objects where weak unblended RLs have been measured with a S/N higher than 10.

In a chemically homogeneous medium $I(\text{O,RL})/I(\text{H,RL})$ is proportional to the O/H ratio and is almost independent of the electron temperature. Alternatively $I(\text{O,CL})/I(\text{H,RL})$ does depend on the electron temperature in such a way that in the presence of temperature variations the O/H abundances derived from temperature determinations based on CLs, assuming constant temperature, yield abundances smaller than the real ones giving rise to the presence of an ADF.

In a chemically inhomogeneous medium CLs are expected to originate mainly in regions that are relatively metal-poor, temperature-high and density-low, while the RLs are expected to originate mainly in regions that are relatively metal-rich, temperature-low, and density-high.

It is the purpose of this paper to study the cause of the ADF values. We will concentrate on the O/H ADF in H II regions considering two options: a) the presence of temperature variations in a chemically homogeneous medium and b) the presence of chemical inhomogeneities. It should be mentioned that chemical inhomogeneities also produce temperature variations. In addition to the evidence in favor of the presence of temperature variations based on chemical abundance determinations there is evidence of temperature variations based on high spatial resolution observations of the Orion nebula and the Ring nebula

(O’Dell et al. 2003, 2013).

The data of H II regions obtained with the Ultraviolet Visual Echelle Spectrograph, UVES, and the very large Kueyen telescope in Chile, VLT are specially suited for the study of faint emission lines due to their high quality, produced by their high spectral resolution and their high S/N. There are nine H II regions that have been observed with this equipment (Peimbert 2003; Esteban et al. 2004; García-Rojas et al. 2004, 2005, 2006, 2007). The observational data already published will be used in this paper. Hereafter we will refer to this data set as the UVES set. These papers show fractions of the spectra presenting the region of multiplet V1 of O II where the spectral resolution and the S/N can be appreciated. With the exception of the densities and temperatures derived in this paper and those derived by McNabb et al. (2013) from the UVES set, all the other values and densities presented in this paper were computed in the original papers that contain the observational UVES set.

In Section 2 we derive the electron temperatures from the ratio of [O III] lines, $T(4363/4959)$, and from the ratio of the sum of the 8 recombination lines of multiplet V1 of O II to the 4959[O III] line, $T(V1/4959)$, and from these values the average temperature and mean square temperature variation of the O^{++} region, $T_0(O II)$ and $t^2(O II)$. We also compare these T_0 and t^2 values with those derived from other forbidden and permitted line ratios, such as those derived from the Balmer lines and continuum. In Section 3 we derive electron densities based on the O II recombination lines and compare them with those derived from forbidden lines. In Section 4 we compare the pressure derived from collisionally excited lines with that derived from recombination lines. In Section 5 we compare the O/H ratio derived with eight different methods for 30 Doradus, an H II region in the Large Magellanic Cloud. The discussion and conclusions are presented in Sections 6 and 7 respectively.

2. Temperature determinations based on the O II and [O III] lines

Earlier calculations of the effective recombination coefficients of O II were derived under the assumption that the fine-structure levels of the ground term of the recombining ion are thermally populated in proportion to their statistical weights (Peimbert et al. 1993; Storey 1994), an assumption that has been shown to be inaccurate under low density nebular conditions (Ruiz et al. 2003; Peimbert & Peimbert 2005).

New ab initio calculations of the effective recombination coefficients, valid down to very low temperatures and taking into account the density dependence of the level populations of the ground states of the recombining ion, are now available for the recombination spectrum of O II (Bastin & Storey 2006; Liu 2012; Fang & Liu 2013, Storey unpublished).

When choosing which O II RLs to use to derive the temperature and the abundance of the O⁺⁺ region there are three strong reasons to use the sum intensities of the eight lines of the V1 multiplet, $I(\text{V1})$: a) V1 is the brightest multiplet in the visual region, b) the intensity of a single line of the V1 multiplet is density dependent and the error in the density determination propagates into the resulting temperature or abundance, while the total intensity of the multiplet is practically density independent, and c) the error in the determination of the intensity of the whole multiplet, if the resolution is high enough to detect all the lines without blends from other ions, is considerably smaller than that of a single line.

The emission coefficients per ion per electron per cm⁻³ for these lines: ε_{V1} , ε_{4959} , and ε_{4363} as a function of temperature in the 5000 to 15000K range are given by:

$$\varepsilon_{\text{V1}}(T_e) = C_{\text{V1}}T_e^{-0.755}, \quad (1)$$

$$\varepsilon_{4959}(T_e) = C_{4959}T_e^{-0.34}\exp(-29160/T_e), \quad (2)$$

and

$$\varepsilon_{4363}(T_e) = C_{4363}T_e^{-0.34}\exp(-62120/T_e), \quad (3)$$

(Lennon & Burke 1994; Mendoza et al. 1999) where the C values are constants that depend on atomic parameters. The observed intensity of each line is given by:

$$I = \int \frac{\varepsilon(T_e)n_en(\text{O}^{++})}{r^2}dV, \quad (4)$$

where V is the emitting volume and r is the distance to the source. If we assume that T_e is constant in the observed volume we have that

$$I = \varepsilon(T_e) \int \frac{n_en(\text{O}^{++})}{r^2}dV = \varepsilon(T_e)W(\text{O}^{++}), \quad (5)$$

where $W(\text{O}^{++})$ is closely related to the emission measure and is common to all O⁺⁺ lines; therefore the ratio of two line intensities only depends on the emissivities, consequently

$$\frac{I(\text{V1})}{I(4959)} = \frac{\varepsilon_{\text{V1}}(T_e)}{\varepsilon_{4959}(T_e)} = R_{(\text{V1}/4959)}(T_e) = \frac{C_{\text{V1}}}{C_{4959}}T_e^{-0.415}\exp(29160/T_e), \quad (6)$$

and

$$\frac{I(4363)}{I(4959)} = \frac{\varepsilon_{4363}(T_e)}{\varepsilon_{4959}(T_e)} = R_{(4363/4959)}(T_e) = \frac{C_{4363}}{C_{4959}}\exp(-32940/T_e), \quad (7)$$

where $R_{(\text{V1}/4959)}$ and $R_{(4363/4959)}$ are the ratios of the emission coefficients; and $C_{\text{V1}}/C_{4959} = 6.56 \times 10^{-5}$ and $C_{4363}/C_{4959} = 0.496$ (Storey 1994; Lennon & Burke 1994; Mendoza et al.

1999). In Figure 1 we present Equation 6, the relation between $R_{(V1/4959)}$ and T_e ; equation 7 is the most often used to determine the temperature of photoionized regions.

From equations 6 and 7 we have determined $T_e(V1/4959)$ and $T_e(4363/4959)$, which, together with the $T(O\ II)$ values derived by McNabb et al. (2013), are presented in Table 1. For all objects of the UVES set we find that $T_e(4363/4959)$ is higher than $T_e(V1/4959)$, considering that the dependence on T_e is stronger for $I(4363/4959)$ than for $I(V1/4959)$, it is possible that the difference between the two sets of temperatures could be due to the presence of temperature variations over the observed volume.

We decided to follow the formalism introduced by Peimbert (1967) to determine the basic parameters of the temperature structure, $T_0(O^{++})$ and $t^2(O^{++})$, where

$$T_0(O^{++}) = \frac{\int T_e n_e n(O^{++}) dV}{\int n_e n(O^{++}) dV}, \quad (8)$$

and

$$t^2(O^{++}) = \frac{\int (T_e - T_0(O^{++}))^2 n_e n(O^{++}) dV}{T_0(O^{++})^2 \int n_e n(O^{++}) dV}. \quad (9)$$

In the presence of temperature variations it is not possible to simplify equation 4 in the way is done in equation 5. In appendix A we present a way to relate line intensity ratios to the temperature structure. In this formalism we need two independent line intensity ratios (of lines of the same ion and with little density dependence) to derive $T_0(O^{++})$ and $t^2(O^{++})$.

From equation A9 and the temperature dependence of ε_{V1} , ε_{4959} , and ε_{4363} (equations 1, 2, and 3) we can write $T_e(V1/4959)$ and $T_e(4363/4959)$ as a function of T_0 and t^2 :

$$T_e(4363/4959) = T_0(O^{++}) \left[1 + \left(\frac{91300}{T_0(O^{++})} - 2.68 \right) \frac{t^2(O^{++})}{2} \right], \quad (10)$$

and

$$T_e(V1/4959) = T_0(O^{++}) \left[1 + \left(\frac{29160}{T_0(O^{++})} - 3.095 + \frac{0.415}{\frac{29160}{T_0(O^{++})} + 0.415} \right) \frac{t^2(O^{++})}{2} \right]. \quad (11)$$

Therefore from equations 10 and 11 we have derived $T_0(O^{++})$ and $t^2(O^{++})$, presented in Tables 1 and 3.

Fang & Liu (2013) and McNabb et al. (2013) have used the $I(4649)/I(4089)$ O II ratio to derive the electron temperature of the O^{++} zone using only recombination lines (where $\lambda\ 4649$ belongs to the V1 multiplet, and $\lambda\ 4089$ belongs to the V48a multiplet). We have decided not to use this ratio for the following reasons: a) $\lambda\ 4089$ has been detected only in

three of the nine H II regions in our sample: 30 Doradus, Orion, and NGC 3576, while for the other six regions only an upper limit to the intensity of the λ 4089 line can be obtained, that corresponds to a lower limit in the temperature, b) the $I(4649)/I(4089)$ ratio depends very weakly on the electron temperature and in the three regions where it has been detected the error in the ratio is in the 15% to 20% range, an error of 15% in the $I(4649/4089)$ O II ratio implies an error of about 3500 K for a temperature of 8000 K, c) λ 4089 can have a significant contribution due to the Si IV line at λ 4088.86, in this case only a lower limit of the temperature can be obtained from the $I(4649)/I(4089)$ ratio.

There is evidence in favor of a contribution to the λ 4089 feature due to the presence of the Si IV line at λ 4088.86 for two of the three regions where λ 4089 has been detected. For the Orion nebula a line around λ 4116.10 has been detected and Esteban et al. (2004) suggested that it might be due to a line of the v2F0-6D multiplet of Fe II] at 4116.067, we do not agree with this suggestion because the other 5 lines of multiplet v2F0-6D were not detected: λ 4030.970, 4065.317, 4131.621, 4184.051 and 4243.085. We suggest that the line at λ 4116.10 is the weaker one of the doublet of Si IV that includes λ 4088.86. To confirm this suggestion we looked again at the original UVES spectrum of the Orion nebula (see Figure 2) and found that indeed the λ 4088.86 line is present with an intensity of 0.017 after correcting for reddening, where $I(H\beta) = 100$. Therefore the observed $I(4088.86)/I(4116.10)$ ratio is equal to 2.4 in good agreement with the theoretical ratio that amounts to two.

Furthermore the presented λ 4088.86, 4089.29, and 4116.10 line intensities are lower limits to the real intensities because in Orion there is a substantial component of the continuum due to dust scattered light (O’Dell & Hubbard 1965) that is expected to show the Si IV lines in absorption. The dust scattered light is mainly due to the brightest stars in the Trapezium with B0.5V, B0V, O7V and O9.5V spectral types, for components A, B, C, and D, respectively (Iriarte et al. 1965; Hoffleit & Jaschek 1982; Conti & Alschuler 1971), the Si IV lines reach their peak intensities around the spectral type O9.5 to B0.5 (Conti 1973; Rudnick 1936). Si IV lines in absorption have been detected in component C of the Trapezium see Figure 4 of Esteban et al. (1998) . We have not estimated the correction due to the underlying absorption that affects the Si IV λ 4088.86 and the O II λ 4089.29 line intensities in emission.

For 30 Doradus, where the feature at λ 4089 has also been detected, there is an additional argument in favor of the presence of the Si IV line based on the central wavelength of the observed feature. The theoretical displacement of the Si IV λ 4088.86 line is 0.43 Å to the blue of the O II line at λ 4089.29. For 30 Doradus the observed feature identified as λ 4089.29 is shifted towards the blue by 0.31 Å relative to the wavelength frame defined by the O II lines at λ 4072.16, and 4078.84, the shift suggests that a substantial fraction of the blend

could be due to Si IV. By assuming that one fifth to two fifths of the $\lambda 4089$ blend is due to Si IV we obtain a temperature in the 5000 to 12600 K range, while by assuming that the $\lambda 4089$ intensity is due only to O II a temperature of 400 K is obtained.

Another argument in favor of the presence of Si IV in gaseous nebulae is that the weaker line of the Si IV doublet at $\lambda 4116.10$ has been detected in some planetary nebulae of intermediate degree of ionization like NGC 6543, NGC 6572, IC 4997 and of higher degree of ionization like NGC 7009 and NGC 7662 (Hyung et al. 2000, 1994a,b; Hyung & Aller 1995; Aller, et al. 1966).

For the other six H II regions of our sample $\lambda 4089$ was not detected, therefore an estimate of the $\lambda 4089$ intensity is only an upper limit of the O II feature and consequently the T_e values derived from Figure 2 of McNabb et al. (2013) (that shows $I(4649)/I(4662)$ and $I(4649)/I(4089)$ as a function of density and temperature) become only lower limits to the real $T(\text{O II})$ value.

From the $T_0(\text{O}^{++})$ values presented in Table 1 we have estimated that, to determine the $\lambda 4089$ line intensity with an error of 15% for the six objects where it was not detected, we need new observations with signal to noise ratios 4 to 13 times better than those present in the UVES set (4 for M8 and 13 for M20).

In Table 1 we also present the temperatures derived by McNabb et al. (2013), from the $I(4649)/I(4089)$ ratio, from the arguments and results presented above we consider that their results are only lower limits to the electron temperature, with the exception of the Orion nebula value that might be an upper limit to the temperature due to the contribution of dust scattered light showing the Si IV line in absorption.

To study the possibility of chemical inhomogeneities we present in Tables 2 and 3 temperatures and mean square temperature variations derived from the O II and [O III] lines by us in this paper, and from the He I and H I lines as well as the Balmer continuum from the UVES set in the literature. From these tables we find similar values for the O, He, and H temperatures and mean square temperature variations in agreement with chemical homogeneity for this group of H II regions.

3. Density determinations based on the O II lines

The electron densities for the H II regions were derived from Figure 3, where we plot the predicted $I(4649)/I(4639 + 4651 + 4662)$ ratio from the atomic data by Storey (unpublished, see also Fang & Liu 2013) and are presented in Table 4. We decided to use this ratio because

the error in the $I(4639 + 4651 + 4662)$ value is smaller than the error in the $I(4662)$ value and the behavior versus density of $I(4639)$ and $I(4651)$ is similar to that of $I(4662)$. The use of Figure 3 requires a temperature, and we are using the $T_0(\text{O II})$ temperature presented in Table 1, derived from the $I(4959)/I(\text{V1})$ and $I(4959)/I(4363)$ ratios that is considerably more accurate than the temperature derived from the $I(4649)/I(4089)$ ratio for the reasons presented in the previous section.

For M20 $I(4639)$ was not measured, and the errors in the determination of $I(4649)$, $I(4651)$, and $I(4662)$ are the largest of the sample and were not estimated, therefore we did not obtain the density for this object.

Also in Table 4 we include the densities derived from CLs presented in the VLT UVES papers. The atomic data used to derive the O II densities from RLs by McNabb et al. (2013) and us is the same, the different results come from the different O II lines used to determine the density and because we used the $I(4959)/I(\text{V1})$ ratio to determine the temperature while McNabb et al. used other O II lines to determine the temperature.

4. Electron pressure in H II regions

We determined the pressures using the ideal gas equation. In Table 5 we present the ratio of the pressure derived from the collisionally excited lines to the pressure derived from the recombination lines, $P(\text{CLs})/P(\text{RLs})$. For $P(\text{CLs})$ we adopted the following equation,

$$P(\text{CLs}) = n_e \langle \text{CLs} \rangle kT_e(4363/4959), \quad (12)$$

where $n_e \langle \text{CLs} \rangle$, the average of the density determinations from CLs, was obtained from the original papers and is presented in Table 4, k is the Boltzmann constant, and $T_e(4363/4959)$ is presented in Table 1. The $P(\text{RLs})$ were obtained from $n_e(\text{O II})$ and $T_0(\text{O}^{++})$. For comparison we also present the ratio of pressures derived from the results by McNabb et al. (2013), where the $P(\text{CLs})$ are the values derived by us and the $P(\text{RLs})$ are the values derived from the densities and temperatures presented in Table 2 of McNabb et al. (2013) (values also presented in the last column of Tables 1 and 4 of this paper).

The pressure ratios derived from our data are in the 0.85 to 3.95 range with an average value of 2.4. We consider that these ratios are important clues to study the process or processes that are responsible for the temperature variations present in H II regions.

In Figure 4 we show the $P(\text{CLs})/P(\text{RLs})$ versus the $n_e(\text{O II})$ values. This figure shows a trend of higher $P(\text{CLs})/P(\text{RLs})$ with higher $n_e(\text{O II})$ values, the lowest density H II regions show pressure ratios close to one, while the high density H II regions show pressure ratios close

to four. A seemingly stronger correlation could be presented by plotting $P(\text{CLs})/P(\text{RLs})$ versus $n_e[\text{Cl III}]$, but it is not more meaningful because $n_e[\text{Cl III}]$ is a positive ingredient in the pressure ratio.

These correlations indicate that there is a mechanism capable of producing hot clumps of high density. Since $P(\text{CLs})/P(\text{RLs})$ is generally higher than one, it follows that hot, rather than cold, high density clumps are the dominant cause of temperature inhomogeneities. Furthermore this correlation shows that the mechanism that produces these hot clumps is more efficient at higher densities than at lower densities. This mechanism might be related with the age of the H II region, (in general we expect younger regions to be denser); it can also be related to shock waves (which would produce hot over-dense regions), that could be driven by turbulence (of which more is expected in young regions).

The $P(\text{CLs})/P(\text{RLs})$ derived from the temperatures and densities obtained from RLs by McNabb et al. (2013) go from 1.32 to 530 with an average value of 89, if we disregard NGC 3603 their average value becomes 34 a value more than one order of magnitude higher than the one derived by us. We consider that the overestimation of the very weak O II line intensities used by McNabb et al. (2013), that is partly due to blends of these lines with even weaker lines, is the main reason for the differences in the derived temperatures and densities.

We decided to compare the radial velocities of the O II and [O III] lines to try to find out if there was any difference that could give us a clue on the study of thermal inhomogeneities. In Table 6 we present the median heliocentric radial velocity of five lines of the V1 multiplet of O II, lines for which their intensity decreases with increasing temperature, and compare them with those of the $\lambda 4363$ [O III] line, which originates in the O^{++} region and whose intensity increases the most with temperature. We did not use the $\lambda 4959$ and $\lambda 5007$ [O III] lines due to two reasons: a) they are less temperature dependent than $\lambda 4363$ and b) their shape might be affected by saturation effects. The average velocity difference between the O II and the [O III] lines of the sample amounts to 0.3 km/s, consistent within the uncertainties. This result is consistent with the idea that the H II regions of the sample are chemically homogeneous.

5. 30 Doradus

It is well known that the abundances derived from collisionally excited lines based on the 4363/5007 [O III] temperatures, the so called direct method, are smaller than those derived from recombination lines. This difference has been known as the abundance discrepancy

factor, ADF, the differences for H II regions are typically of about a factor of 1.5 to 3. The ADF values pose two fundamental problems: a) which are the correct abundances, and b) which are the physical conditions responsible for the difference in the derived abundances.

We will use 30 Doradus to advance further on this problem. 30 Doradus is a bright well observed H II region that has most of its oxygen in the twice ionized state. From the UVES observations it amounts to 85%, therefore its O/H ratio is one of the best studied among the observed galactic and extragalactic H II regions. From the observations of 30 Doradus by Peimbert (2003) there are at least eight qualitatively different determinations of the O/H ratio that can be obtained. In what follows we will present these determinations that exemplify some of the main methods that have been used to determine the O/H ratios in gaseous nebulae. We will discuss them in order of the derived O/H ratio.

The eight types of determinations that we will consider are: 1) Direct method (DM), 2) method based on the [O II] and [O III] nebular line intensities taking into account the degree of ionization and calibrated with DM abundances (Pilyugin & Thuan 2005) 3) chemically homogeneous photoionization model (Tsamis & Péquignot 2005), 4) chemically inhomogeneous photoionization model (Tsamis & Péquignot 2005), 5) recombination lines method (RL), 6) RL method plus the contribution to the O/H ratio due to the fraction of O tied up in dust grains, 7) method based on the intensity of the λ 4363 [O III] auroral line of a given object and the calibration by Peña-Guerrero et al.(2012) based on RL abundances including the fraction of O tied up in dust grains, CALM method (Calibration based on the Auroral Lines Method), and 8) method based on the intensity of the λ 3727 [O II] and λ 5007 [O III] nebular lines and the calibration by Peña-Guerrero et al.(2012) based on O II RL abundances including the fraction of O tied up in dust grains, RRM method (Revised R_{23} Method).

In Table 7 we present the eight O/H determinations. The DM method is based on the assumption of $t^2 = 0.00$ and the adoption of the temperatures derived from the ratio of the auroral and nebular lines of [O II] and [O III]. S1 is the homogeneous photoionization model computed by Tsamis & Péquignot (2005), this model produces small temperature fluctuations that increase the O/H ratio by 0.03 dex relative to the value derived with the DM. Since the homogeneous photoionization model fails to reproduce the RLs of O II, Tsamis & Péquignot (2005) presented an inhomogeneous photoionization model with O rich low temperature clumps embedded into an H II region with normal O abundances, the D2 model. This model adjusts properly many of the observed CLs and RLs intensities and leads them to two conclusions: a) the temperature variations could be explained by the presence of the O-rich (O/H = 9.30) low temperature clumps, and b) if this is the case, the overall abundance of 30 Doradus is intermediate between those derived from CLs and RLs. The O/H

gaseous abundance derived from the RL method is almost independent of the temperature, and the difference between the RL and DM methods is due to the temperature structure in the nebula. The RL plus dust method takes into account the fraction of O atoms tied up in dust grains (Peimbert & Peimbert 2010). Finally the gas plus dust O/H ratios based on the CALM and RRM calibrations are also presented in Table 7. These last two methods were calibrated using determinations based on the RLs plus dust method, so we expect the last 3 methods to agree within errors.

We consider that the best abundances for 30 Doradus, and for other H II regions, are those given by the RL + dust method. If the RLs are not available for a given object, but the auroral lines are, the best determination is that given by CALM and if only the nebular lines are available the best determination is the one given by the RRM.

In Table 8 we also include the t^2 values and the average T_0 values for the H⁺ and O⁺⁺ zones predicted by the inhomogeneous photoionization model by Tsamis & Péquignot (2005) and the values derived from observations under the assumption of chemical homogeneity.

6. Discussion

The ADF problem comes from trying to reconcile the abundances derived from forbidden lines with those derived from recombination lines. The ADF problem is present in planetary nebulae and in H II regions. The ADF values in PNe can be due to four causes: temperature variations, chemical inhomogeneities, strong density variations, and non Maxwellian electron velocity distributions. For some objects it is not easy to separate these causes, for example chemical inhomogeneities produce temperature variations. For chemically homogeneous nebulae the proper abundances are those given by RLs, while in the presence of chemical inhomogeneities the representative abundances are intermediate between RL and CL abundances.

Chemical inhomogeneities in some PNe are well established (e.g. Jacoby 1979; Jacoby & Ford 1983; ?; Hazard et al. 1980; Torres-Peimbert et al. 1990; Liu et al. 2000; Barlow et al. 2006), and probably they are the dominant component of the ADF values higher than about 5, we consider that most PNe with ADF values smaller than about 5 are probably chemically homogeneous. See the review by Liu (2006) discussing evidence in favor of chemical inhomogeneities in PNe, and the review by Peimbert & Peimbert (2006) discussing evidence in favor of chemical homogeneity for most PNe with ADF values smaller than about 5.

The effect of electron densities on the abundance determinations of gaseous nebulae can also mimic spurious ADF values. Rubin (1989); Viegas & Clegg (1994); Tsamis et al. (2011)

have studied the dependence of the line intensities on density when the upper energy levels producing forbidden lines are de-excited by collisions. Depending on the line of a given ion the critical density for collisional de-excitation is different. If this effect is not taken into account the temperatures derived from CLs are overestimated and the abundances are underestimated. This can be the case for high density gaseous nebulae and for certain ions. This effect is particularly relevant when infrared lines are used to determine abundances and for objects of relatively high density. We do not expect this effect to be important for the objects studied in this paper, since we are mainly using the 4363 and 4959 [O III] lines that have critical densities of 2.4×10^7 and $6.4 \times 10^5 \text{ cm}^{-3}$ respectively, values that are considerably higher than the densities of the H II regions considered here.

Stasińska et al. (2007) have discussed the possibility that the ADF might be due to the presence of metal rich droplets inside H II regions. Their model predicts that the n_d/n_{HII} ratio is approximately ten, where n_d is the density in the droplets and n_{HII} is the density in the ambient H II region. Since in this model most of the recombination line emission is expected to come from the metal-rich droplets and most of the collisionally excited line emission is expected to originate from the ambient H II region a ratio of $n(\text{O II})/n\langle CL \rangle$ considerably higher than one is expected. From Table 4 we obtain that for the UVES sample the average $n(\text{O II})/n\langle CL \rangle$ is approximately 0.5 which is in conflict with the high metallicity droplets model.

Tsamis & Péquignot (2005) have presented a photoionization model with two components, a component made of metal rich inclusions of low temperature and high density in pressure equilibrium with the other component. They adopt equal pressures for both components at similar optical depths. For an increasing metallicity of the clumped component its electron temperature decreases due to the more efficient cooling from CELs, while because of the equal pressures, its electron density proportionally increases. The idea of taking into account the behavior of the pressure in a two component model is an excellent tool to study the possible presence of metal rich inclusions of low temperature and high density. We will come back to this idea further on.

Nicholls et al. (2012) have suggested that electrons do not have time to thermalize in ionized nebulae so κ -distributions are better suited than Maxwellian distributions to represent the electron distributions in these objects. A κ -distribution can be represented by a t^2 value, for objects with $\kappa > 10$ by the following relation:

$$t^2 = 0.96/\kappa, \quad (13)$$

this relation is obtained from equations 16 and 18 of Peimbert (1967), and figure 10 of Nicholls et al. (2012). The accuracy of the equation is better than 1% in the 5000 to 20000 K temperature range.

We prefer the use of t^2 instead of κ for the following reasons: a) the t^2 formalism applies to many energy distributions for the electrons, not only to κ -distributions; b) t^2 can be used for objects with volume elements with different Maxwellian distributions (different temperatures), as well as objects with volume elements with different κ -distributions; c) to use κ -distributions, the processes that produce these distributions need to dominate the processes that produce Maxwellian distributions, while the t^2 formalism can be used for nebulae with Maxwellian distributions that include perturbations due to κ -distributions, d) κ -distributions have an excess of fast electrons (when compared with a single Maxwellian distribution) but no excess of slow electrons, and thus can only represent a limited number of physical processes, in particular they can not represent physical mechanisms that produce cooler regions, e.g. shadow ionization, while the t^2 formalism allows for processes that produce hotter and/or cooler regions, e) t^2 values predicted by photoionized models make non negligible contributions to the t^2 observed values, these contributions cannot be fitted by κ -distributions.

Peña-Guerrero et al. (2012) present a list of 28 Galactic and extragalactic H II regions with accurate t^2 determinations. The average ADF for this set is 1.7, while the average t^2 value is 0.044. From Equation 13 this t^2 value corresponds to a κ of 22.

The best O II recombination lines to derive the electron temperature and the electron density are those of multiplet 1, and the best observations available are those of the UVES set, obtained with the echelle of the VLT. The error in the temperature derived from the $I(4649)/I(4089)$ ratio of O II is considerably higher than the error in the temperature derived from the $I(4959,[O III])/I(V1,O II)$ ratio. The reasons are: a) $\lambda 4089$ is a very weak line (moreover other O II lines that can be used to obtain the $T_e(O II)$ value, e.g. 4189 and 4590, are expected to be at least a factor of three weaker than 4089), b) $\lambda 4089$ is blended with other weak lines in particular with Si IV at $\lambda 4088.85$, c) the dependence of the temperature on the $I(4649)/I(4089)$ ratio is very weak; we conclude from this discussion that higher signal to noise data to that of the UVES set is needed to derive the temperature based only on recombination lines. Alternatively: a) $\lambda 4959$ is a very strong line, b) $\lambda 4959$ is not blended with lines of significant intensity, c) the $I(4959,[O III])/I(V1,O II)$ ratio depends strongly on the temperature, d) in observations with the quality of the UVES set the lines of multiplet V1 are not blended with other lines, as can be seen in the figures of this multiplet presented in the UVES papers and in the agreement between the observed wavelengths with the theoretical ones.

In this paper we derive an equation based on the new recombination computations for O II by Storey (unpublished, but available from: Liu 2012; McNabb et al. 2013; Fang & Liu 2013) to derive T_e from the ratio of [O III] to O II lines. We compare this temperature with

the $T_e(4363/5007)$ temperature and obtain $t^2(\text{O}^{++})$ values that are in very good agreement with the $t^2(\text{He}^+)$ values derived from comparing of $T_e(\text{He I})$ to $T_e(4363/4959)$, and with the $t^2(\text{He}^+)$ values derived from comparing the temperature determined from H I recombination lines and the Balmer continuum, $T_e(\text{Bac})$ to $T_e(4363/5007)$. The agreement among the three types of t^2 values implies that in these objects H, He, and O are well mixed or, in other words, that these objects are chemically homogeneous and that there are no high density low temperature knots inside the H II regions of the UVES set. Moreover the $T_0(\text{O}^{++})$, $T_0(\text{He}^+)$, and $T_0(\text{H}^+)$ values for a given object are similar. These results imply that the H II regions of our sample are chemically homogeneous and that the ADF values are due to temperature variations, that the O/H abundances derived from recombination lines of O and H represent the correct O/H values. Other arguments in favor of the RL abundances have been presented elsewhere (Peimbert & Peimbert 2011; Simón-Díaz & Stasińska 2011).

From Figure 3 and the line intensities of the UVES set we derive the density of the H II region based only on O II recombination lines and find that it is similar or lower than the density derived from forbidden lines, this result also implies that the O II lines do not originate in high density knots. Moreover the electron pressure derived from the O II densities is similar to the electron pressure derived from the forbidden line densities. The small pressure differences between the recombination lines and the forbidden lines might be giving us clues about the cause of the temperature variations.

Following the idea of the two components model one would expect the pressure derived from the CLs to be similar to the pressure derived from the RLs. A study using the recombination lines of O II and N II to determine temperatures and densities was made by McNabb et al. (2013) for a large number of PNe and H II regions. In Table 5 we present the ratio of the pressures from the O II lines derived from their Table 2 and those derived in this paper and find very large differences. From the temperatures and densities derived by McNabb et al. (2013) we obtain an average $P(\text{CLs})/P(\text{RLs})$ higher than 34 for the nine H II regions discussed in this paper (see Table 4). This result, if taken at face value, is contrary to the idea that there are high density low temperature knots embedded in these gaseous nebulae.

McNabb et al. (2013) have in common with us five objects where they were able to determine temperatures and densities from RLs of both N^{++} and O^{++} , these results are presented in their Table 2. The objects are M8, M17, NGC 3576, Orion, and 30 Doradus. From the ideal gas equation and the data presented by McNabb et al. (2013) it is found that the N II to O II electron pressure ratio, $P(\text{N II})/P(\text{O II})$, presents a range of six orders of magnitude: from a ratio of 0.035 for the Orion nebula to a ratio of 50,000 for 30 Doradus. Since we expect the O^{++} and N^{++} regions to overlap substantially we expect the measured

electron pressure ratio to be close to one. We consider that a large fraction of the range in the electron pressure ratio is due to large errors in the measurement of the recombination line intensities.

From the results of this paper, see Table 4, we obtain an average for $P(\text{CLs})/P(\text{RLs})$ for 8 H II regions equal to 2.4. This result also indicates that there are no metal-rich, high-density, low-temperature knots present in our sample. Moreover this result is significantly larger than 1.0 and might give us a clue to explain the mechanism or mechanisms that produce the temperature variations. This value implies that the regions where the CLs mainly originate have slightly higher densities and temperatures than the regions where the RLs mainly originate; these pressure differences might be due to mild shocks or magnetic reconnection.

7. Conclusions

We present a set of equations and figures to derive $T(\text{V1}/4959)$, t^2 (O II), and T_0 (O⁺⁺), based only on forbidden and permitted lines of the O⁺⁺ region.

The average temperatures and t^2 values derived from $T(4363/4959)$ and $T(\text{V1}/4959)$ are in very good agreement with the t^2 values derived from H and He recombination lines. Moreover the $T_0(\text{O}^{++})$, $T_0(\text{He}^+)$, and $T_0(\text{H}^+)$ values are similar. These results imply that the H II regions of our sample are chemically homogeneous. Or in other words that H, He and O are well mixed in H II regions, that the ADF values are due to temperature variations, and that the O/H abundances derived from recombination lines of O and H represent the correct O/H values.

The densities derived from the recombination lines of multiplet 1 of O II of our sample are in agreement with or smaller than the densities derived from the forbidden lines. The average pressure for the H II regions of the sample derived from [O III] collisionally excited lines is a factor of 2.4 higher than the pressure derived from O II recombination lines. This difference might be significant. If this is the case it might be giving us information on the mechanism or mechanisms that produce the large observed t^2 values.

We present evidence against the presence of metal-rich, temperature-low, density-high inclusions in the H II regions studied in this paper.

Of the several methods used to obtain the O/H ratio in H II regions we consider the RL + dust to be the best one. The second best is the one based on auroral lines but corrected taking into account t^2 , dust and the ionization structure, CALM method (Calibration based on the

Auroral Lines Method). The third best is the one based on nebular lines but corrected taking into account t^2 , dust and the ionization structure, RRM method (Revised R₂₃ Method). The direct method provides only a lower limit to the real O/H value.

We are grateful to an anonymous referee for a critical reading of the manuscript. We are also grateful to Gary Ferland, Jorge García-Rojas, and María de los Ángeles Peña-Guerrero for fruitful discussions. We received partial support from PAPIIT grant IN291129 and from CONACyT grant 129753.

A. Line intensity ratios in the presence of temperature variations

H II regions have, in general, a temperature structure; for each ion present in the ionized region it is possible to use equations equivalent to equation 8 to determine $T_0(ion)$, as well as equations equivalent to equations 5 and 9, to derive $W(ion)$ and $t^2(ion)$.

When trying to estimate the intensity of a line $I(\lambda)$ as a function of its emission coefficient in the presence of temperature variations, it is not possible to factorize $\varepsilon(T_e)$ from integrals like the one in equation 4: since T_e is not constant, $\varepsilon(T_e)$ won't be either; the solution proposed by (Peimbert 1967) lies in expanding $\varepsilon(T_e)$ as a Taylor series around $T_0(ion)$:

$$\varepsilon(T_e) = \varepsilon(T_0(ion)) + \frac{(T_e - T_0(ion))}{1!} \frac{d\varepsilon}{dT}(T_0(ion)) + \frac{(T_e - T_0(ion))^2}{2!} \frac{d^2\varepsilon}{dT^2}(T_0(ion)) + \dots \quad (\text{A1})$$

from equations 4 and A1 we obtain:

$$I = \int \frac{\varepsilon(T_0(ion))n_en(ion)}{r^2} dV + \int \frac{\varepsilon'(T_0(ion))(T_e - T_0(ion))n_en(ion)}{r^2} dV + \frac{1}{2} \int \frac{\varepsilon''(T_0(ion))(T_e - T_0(ion))^2 n_en(ion)}{r^2} dV + \dots (\text{A2})$$

where ε' and ε'' are the first and second derivatives of ε with respect to T , and can be factored out of the integrals. The remaining integrals are related to $W(ion)$, $T_0(ion)$, and $t^2(ion)$ respectively and equation A2 can be written as:

$$I = \varepsilon(T_0(ion))W(ion) + \varepsilon'(T_0(ion))(T_0(ion) - T_0(ion))W(ion) + \frac{1}{2}\varepsilon''(T_0(ion))t^2(ion)W(ion) + \dots \quad (\text{A3})$$

The term associated with ε' will disappear since we chose to expand the Taylor series around the average temperature, however the term associated with ε'' will not vanish; for moderate thermal inhomogeneities the contribution of the second order term will be much more important than higher order terms which we will ignore, therefore

$$I = \varepsilon(T_0(ion))W(ion) \left[1 + \left(\frac{T_0(ion)^2 \varepsilon''(T_0(ion))}{\varepsilon(T_0(ion))} \right) \frac{t^2(ion)}{2} \right]. \quad (\text{A4})$$

When considering the ratio of the intensities of two lines originating from the same ion (the line intensities should have little or no density dependence), we obtain

$$\frac{I(\lambda_1)}{I(\lambda_2)} = \frac{\varepsilon_1(T_0(\text{ion}))}{\varepsilon_2(T_0(\text{ion}))} \left[\frac{1 + \left(\frac{T_0(\text{ion})^2 \varepsilon_1''(T_0(\text{ion}))}{\varepsilon_1(T_0(\text{ion}))} \right) \frac{t^2(\text{ion})}{2}}{1 + \left(\frac{T_0(\text{ion})^2 \varepsilon_2''(T_0(\text{ion}))}{\varepsilon_2(T_0(\text{ion}))} \right) \frac{t^2(\text{ion})}{2}} \right]. \quad (\text{A5})$$

In the regime of small temperature variations we obtain that

$$\frac{I(\lambda_1)}{I(\lambda_2)} = R_{\lambda_1/\lambda_2}(T_0(\text{ion})) \left[1 + T_0(\text{ion})^2 \left(\frac{\varepsilon_1''(T_0(\text{ion}))}{\varepsilon_1(T_0(\text{ion}))} - \frac{\varepsilon_2''(T_0(\text{ion}))}{\varepsilon_2(T_0(\text{ion}))} \right) \frac{t^2(\text{ion})}{2} \right]. \quad (\text{A6})$$

This shows that when using an uncorrected $R_{\lambda_1/\lambda_2}(T) = \varepsilon_1/\varepsilon_2$ to determine the temperature from the $I(\lambda_1)/I(\lambda_2)$ ratio, the determination will be skewed. To correct for the presence of temperature variations over the observed volume we have that

$$\begin{aligned} \frac{I(\lambda_1)}{I(\lambda_2)} = R_{\lambda_1/\lambda_2}(T) &= R_{\lambda_1/\lambda_2}(T_0 + \Delta T) \\ &\approx R_{\lambda_1/\lambda_2}(T_0) + \Delta T R'_{\lambda_1/\lambda_2}(T_0) \\ &\approx R_{\lambda_1/\lambda_2}(T_0) \left(1 + \Delta T \frac{R'_{\lambda_1/\lambda_2}(T_0(\text{ion}))}{R_{\lambda_1/\lambda_2}(T_0(\text{ion}))} \right); \end{aligned} \quad (\text{A7})$$

therefore

$$\begin{aligned} \Delta T \frac{R'_{\lambda_1/\lambda_2}(T_0(\text{ion}))}{R_{\lambda_1/\lambda_2}(T_0(\text{ion}))} &= \Delta T \left(\frac{\varepsilon_1'(T_0(\text{ion}))}{\varepsilon_1(T_0(\text{ion}))} - \frac{\varepsilon_2'(T_0(\text{ion}))}{\varepsilon_2(T_0(\text{ion}))} \right) \\ &= T_0(\text{ion})^2 \left(\frac{\varepsilon_1''(T_0(\text{ion}))}{\varepsilon_1(T_0(\text{ion}))} - \frac{\varepsilon_2''(T_0(\text{ion}))}{\varepsilon_2(T_0(\text{ion}))} \right) \frac{t^2(\text{ion})}{2} \end{aligned} \quad (\text{A8})$$

and finally

$$T_{\lambda_1/\lambda_2} = T_0(\text{ion}) \left[1 + T_0(\text{ion}) \left(\frac{\frac{\varepsilon_1''(T_0(\text{ion}))}{\varepsilon_1(T_0(\text{ion}))} - \frac{\varepsilon_2''(T_0(\text{ion}))}{\varepsilon_2(T_0(\text{ion}))}}{\frac{\varepsilon_1'(T_0(\text{ion}))}{\varepsilon_1(T_0(\text{ion}))} - \frac{\varepsilon_2'(T_0(\text{ion}))}{\varepsilon_2(T_0(\text{ion}))}} \right) \frac{t^2(\text{ion})}{2} \right]; \quad (\text{A9})$$

this equation relates the measured temperature to the average temperature T_0 and to the temperature variations parameter $t^2(\text{ion})$; observationally it means one measurement for two unknowns. If one wants to determine $T_0(\text{ion})$ and $t^2(\text{ion})$ one requires either two independent measurements of the temperature of a single ion (i.e. the measurement of at least 3 lines with different temperature dependence), or two determinations of temperatures for two ions that occupy the same volume.

REFERENCES

- Aller, L. H., Kaler, J. B., & Bowen, I. S. 1966, *ApJ*, 144, 291
- Bastin, R. J. & Storey, P. J. 2006, *Planetary Nebulae in our Galaxy and Beyond (IAU Symp. 234)*, ed. R. H. Méndez and M. J. Barlow (Cambridge: Cambridge Univ. Press), 369
- Barlow, M. J., Hales, A. S., Storey, P. J., Liu, X.-W., Tsamis, Y. G., & Aderin, M. E. 2006, *Planetary Nebulae in our Galaxy and Beyond (IAU Symp. 234)*, ed. R. H. Méndez and M. J. Barlow (Cambridge: Cambridge Univ. Press), 367
- Conti, P. S. 1973, *ApJ*, 179, 171
- Conti, P. S. & Alschuler, W. 1971, *ApJ*, 179, 161
- Esteban, C., García-Rojas, J., Peimbert, M., et al. 2005, *ApJ*, 618, L95
- Esteban, C., Peimbert, M., García-Rojas, J., et al. 2004, *MNRAS*, 355, 229
- Esteban, C., Peimbert, M., Torres-Peimbert, & Escalante, V. 1998, *MNRAS*, 295, 401
- Fang, X. & Liu, X.-W., 2013, *MNRAS*, 429, 2791
- García-Rojas, J., Esteban, C., Peimbert, A., et al. 2005, *MNRAS*, 362, 301
- García-Rojas, J., Esteban, C., Peimbert, A., et al. 2007, *RevMexAA*, 43, 3
- García-Rojas, J., Esteban, C., Peimbert, M., et al. 2006, *MNRAS*, 368, 253
- García-Rojas, J., Esteban, C., Peimbert, M., et al. 2004, *ApJ*, 153, 501
- Hazard, C., Terlevich, R., Ferland, G., Morton, D. C., & Sargent, W. L. W. 1980, *Nature*, 285, 463
- Hoffleit, D. & Jaschek, C. 1982, *The Bright Star Catalogue (New Haven:Yale Univ. Observatory)*
- Hyung, S. & Aller, L. H. 1995, *MNRAS*, 273, 973
- Hyung, S., Aller, L. H., & Feibelman, W. A. 1994a, *MNRAS*, 269, 975
- Hyung, S., Aller, L. H., & Feibelman, W. A. 1994b, *ApJS*, 93, 465
- Hyung, S., Aller, L. H., Feibelman, W. A., Lee, W. B., & de Koter, A. 2000, *MNRAS*, 318,

- Iriarte, B., Johnson, H. L., Mitchell, R. I., & Wisniewski, W. K. 1965, *S&T*, 30, 21
- Jacoby, G. H. 1979, *PASP*, 91, 754
- Jacoby, G. H. & Ford, H.C. 1983, *ApJ*, 266, 298
- Lennon, D. J. & Burke, V. M. 1994, *A&AS*, 103, 273
- Liu, X. 2006, *Planetary Nebulae in our Galaxy and Beyond (IAU Symp. 234)*, ed. R. H. Méndez and M. J. Barlow (Cambridge: Cambridge Univ. Press), 219
- Liu, X. 2012, *Planetary Nebulae: An Eye to the Future (IAU Symp. 283)*, eds. A. Manchado, L. Stanghellini & D. Schönberner (Cambridge: Cambridge Univ. Press), 131
- Liu, X.-W., Storey, P. J., Barlow, M. J., Danziger, I. J., Cohen, M., & Bryce, M. 2000 *MNRAS*, 312, 585
- McNabb, I. A., Fang, X., Liu, X.-W., Bastin, R. J., & Storey, P. J. 2013, *MNRAS*, 428, 3443
- Mendoza, C. Zeippen, C. J., & Storey, P. J. 1999, *A&AS*, 135, 159
- Nicholls, D. C., Dopita, M. A., & Sutherland, R. S. 2013, *ApJ*, 752, 148
- O'Dell, C. R., Ferland, G. Henney, W., & Peimbert, M. 2013, *AJ*, 145, 93
- O'Dell, C. R. & Hubbard, W. B. 1965, *ApJ*, 142, 591
- O'Dell, C. R., Peimbert, M., & Peimbert, A. 2003, *AJ*, 125, 2590
- Peimbert, A. 2003, *ApJ*, 584, 735
- Peimbert, A. & Peimbert, M. 2005, *RevMexAA(SC)*, 23, 9
- Peimbert, A. & Peimbert, M. 2010, *ApJ*, 724, 791
- Peimbert, M. 1967, *ApJ*, 150, 825
- Peimbert, A. & Peimbert, M. 2010, *Planetary Nebulae in our Galaxy and Beyond (IAU Symp. 234)*, ed. R. H. Méndez and M. J. Barlow (Cambridge: Cambridge Univ. Press), 227
- Peimbert, M. & Peimbert, A. 2011, *RevMexAA(SC)*, 39, 1
- Peimbert, M., Peimbert, A., Ruiz, M. T., & Esteban, C. 2004, *ApJS*, 150, 431
- Peimbert, M., Storey, P. J., & Torres-Peimbert, S. 1993, *ApJ*, 414, 626

- Peña-Guerrero, M. A., Peimbert, A., & Peimbert, M. 2012, *ApJ*, 756, L14
- Pilyuging, L. S. & Thuan, T. X. 2010, *ApJ*, 631, 231
- Rubin, R. H. 1989, *ApJS*, 69, 897
- Rudnick, P. 1936, *ApJ*, 83, 439
- Ruiz, M. T., Peimbert, A., Peimbert, M., & Esteban, C. 2003, *ApJ*, 595, 247
- Simón-Díaz, S. & Stasińska, G. 2011, *A&A*, 526, A48
- Stasińska, G., Tenorio-Tagle, G., Rodríguez, M., & Henney, W. J. 2007, *A&A*, 471, 193
- Storey, P. J. 1994, *A&A*, 282, 999
- Torres-Peimbert, S., Peimbert, M., & Pena, M. 1990, *A&A*, 233, 540
- Tsamis, Y. G., Walsh, J. R., Vílchez, J. M., & Péquignot, D. 2011, *MNRAS*, 412, 1367
- Tsamis, Y. G. & Péquignot, D. 2005, *MNRAS*, 364, 687
- Viegas, S. M. & Clegg, R. E. S. 1994, *MNRAS*, 271, 993

Table 1. Temperatures from O II and [O III] lines

Object	$T(4363/4959)^a$	$T(V1/4959)^b$	$T_0(O^{++})^b$	$T(4649/4089)^c$
M16	7650 ± 250	6295 ± 135	6067 ± 167	1000^{+350}_{-460}
M8	8090 ± 140	6756 ± 84	6563 ± 102	1400^{+1600}_{-400}
M17	8020 ± 170	6948 ± 107	6805 ± 127	4000^{+6500}_{-1300}
M20	7800 ± 300	6678 ± 275	6513 ± 328	≤ 400
NGC 3576	8500 ± 50	7238 ± 60	7085 ± 72	3160^{+550}_{-300}
Orion	8300 ± 40	7590 ± 41	7518 ± 47	15800^{+2400}_{-2600}
NGC 3603	9060 ± 200	7612 ± 215	7462 ± 251	7400^{+10}_{-10}
S311	9000 ± 200	7877 ± 230	7777 ± 261	≤ 400
30 Doradus	9950 ± 60	8902 ± 104	8860 ± 113	≤ 400

^aValues from the VLT UVES papers.

^bThis paper.

^cMcNabb et al. (2013) from O II lines.

Table 2. Other temperatures from the literature^a

Object	$T_0(\text{He}^+)$	$T(\text{Bac})$	$T_0(\text{H}^+)$
M16	7300 ± 350	5450 ± 820	5840 ± 880
M8	7650 ± 200	7100 ± 1100	7620 ± 1180
M17	7450 ± 200	$6500 \pm 1000^{\text{b}}$	6890 ± 1060
M20	7650 ± 300	6000 ± 300	6310 ± 330
NGC 3576	6800 ± 400	6650 ± 750	7110 ± 800
Orion	...	7900 ± 600	8290 ± 630
NGC 3603	8480 ± 200	$6900 \pm 1100^{\text{b}}$	7400 ± 1180
S311	8750 ± 500	≤ 10000	≤ 10700
30 Doradus	...	9220 ± 350	9640 ± 370

^aValues from the VLT UVES papers.

^b $T_e(\text{Paschen})$

Table 3. Temperature variations

Object	$t^2(\text{O}^{++})^{\text{a}}$	$\langle t^2 \rangle^{\text{b}}$	$t^2(\text{He I/CL})^{\text{b}}$	$t^2(\text{H I/CL})^{\text{b}}$
M16	0.042 ± 0.007	0.039 ± 0.006	0.017 ± 0.013	0.045 ± 0.014
M8	0.041 ± 0.008	0.040 ± 0.004	0.046 ± 0.009	0.022 ± 0.015
M17	0.033 ± 0.005	0.033 ± 0.005	0.027 ± 0.014	0.035 ± 0.021
M20	0.035 ± 0.012	0.029 ± 0.007	0.017 ± 0.010	0.049 ± 0.019
NGC 3576	0.039 ± 0.003	0.038 ± 0.009	...	0.037 ± 0.017
Orion	0.022 ± 0.002	0.028 ± 0.006	0.022 ± 0.002	$> 0.018 \pm 0.018$
NGC 3603	0.045 ± 0.008	0.040 ± 0.008	0.032 ± 0.014	0.056 ± 0.023
S311	0.035 ± 0.008	0.038 ± 0.007	0.034 ± 0.010	$> 0.010 \pm 0.024$
30 Doradus	0.032 ± 0.004	0.033 ± 0.005	0.033 ± 0.005	0.022 ± 0.007

^aThis paper.

^bValues from the VLT UVES papers.

Table 4. Electron densities (cm^{-3})

Object	$n_e[\text{Cl III}]^a$	$n_e \langle \text{CLs} \rangle^a$	$n_e(\text{O II})^b$	$n_e(\text{O II})^c$
M16	1370 ± 1000	1120 ± 220	660 ± 230	400^{+3600}_{-160}
M8	2100 ± 700	1800 ± 350	560 ± 130	320^{+100}_{-150}
M17	≤ 630	470 ± 120	525 ± 140	200^{+460}_{-100}
M20	350^{+780}_{-350}	270 ± 60	≤ 100
NGC 3576	3500 ± 800	2800 ± 400	950 ± 70	560^{+330}_{-140}
Orion	9400 ± 1000	8900 ± 200	3300 ± 350	3550 ± 1000
NGC 3603	5600^{+3900}_{-2400}	5150 ± 750	1600 ± 650	220^{+15}_{-40}
S311	...	310 ± 80	420 ± 230	≤ 100
30 Doradus	270 ± 240	300 ± 100	355 ± 85	≤ 100

^aValues from the VLT UVES papers.

^bThis paper.

^cMcNabb et al. (2013).

Table 5. Pressure ratios from CLs to RLs

Object	$P(\text{CLs})^a / P(\text{RLs})^a$	$P(\text{CLs})^a / P(\text{RLs})^b$
M16	2.14 ± 0.86	$21.6^{+22.0}_{-19.3}$
M8	3.96 ± 1.19	$32.5^{+85.0}_{-24.0}$
M17	1.06 ± 0.39	$4.70^{+13.3}_{-3.3}$
M20	...	≥ 52.6
NGC 3576	3.54 ± 0.57	$13.5^{+6.0}_{-5.8}$
Orion	2.98 ± 0.33	$1.32^{+0.80}_{-0.40}$
NGC 3603	3.91 ± 1.68	530^{+135}_{-46}
S311	0.85 ± 0.52	≥ 69.7
30 Doradus	0.95 ± 0.38	≥ 74.6

^aThis paper

^bMcNabb et al. (2013).

Table 6. Radial velocities^a

Object	(O II) ^b	[O III] ^c	difference
M16	+4.3±2.9	+3.4±1.0	-0.9±3.1
M8	-9.0±2.2	-6.2±1.0	+2.8±2.4
M17	+7.6±1.8	+5.5±1.0	-2.1±2.1
M20	+3.9±2.7	-0.7±1.0	-4.6±2.9
NGC 3576	-19.0±3.0	-16.9±1.0	+2.1±3.2
Orion	+12.9±1.2	+14.4±0.7	+1.5±1.4
NGC 3603	+15.1±2.7	+15.8±1.0	+0.7±2.9
S311	+64.2±2.3	+66.0±1.0	+1.8±2.5
30 Doradus	+231.1±1.6	+232.6±0.7	+1.5±1.7

^aHeliocentric radial velocities from the UVES set in km/sec.

^b $\lambda\lambda$ 4639,4642,4649,4651, and 4662 lines.

^c λ 4363 line.

Table 7. O/H Values for 30 Doradus

Model	Components	$12 + \log(\text{O}/\text{H})$	ADF
Obs., Direct Method ^a	gas	8.33 ± 0.02	0.00
Cal., Pagel’s Method ^b	gas	8.33 ± 0.05	0.00
Mod., Homogeneous (S1)	gas	8.36 ± 0.03	0.03
Mod., Two-zone (D2)	gas	8.45 ± 0.05	0.12
Obs., Recombination Lines	gas	8.54 ± 0.06	0.21
Obs., RL+dust	gas+dust	8.63 ± 0.06	0.30
Cal., CALM	gas+dust	8.64 ± 0.07	0.31
Cal., RR ₂₃ M	gas+dust	8.68 ± 0.08	0.35

^aDirect method, T assumed to be constant and given by the $I(4363)/I(4959)$ ratio, consequently $t^2(\text{O}^{++}) = 0.000$ and $T_0(\text{O}^{++}) = T(4363/4959)$.

^bPagel’s Method is usually calibrated using the direct method.

Table 8. Average temperatures and t^2 values for 30 Doradus

Model	$T_0(\text{H}^+)$	$T_0(\text{O}^{++})$	$t^2(\text{Bac})$	$t^2(\text{O}^{++})$
Obs., Direct Method ^a	...	9950 ± 60	...	0.000
Mod., Homogeneous (S1) ^b	9962	9818	0.0045	0.003
Mod., Two-zone (D2) ^b	9654	8679	0.0223	0.078
Obs., Recombination Lines ^a	9640	9300	0.022 ± 0.007	0.038 ± 0.005

^aPeimbert (2003).

^bTsamis & Péquignot (2005).

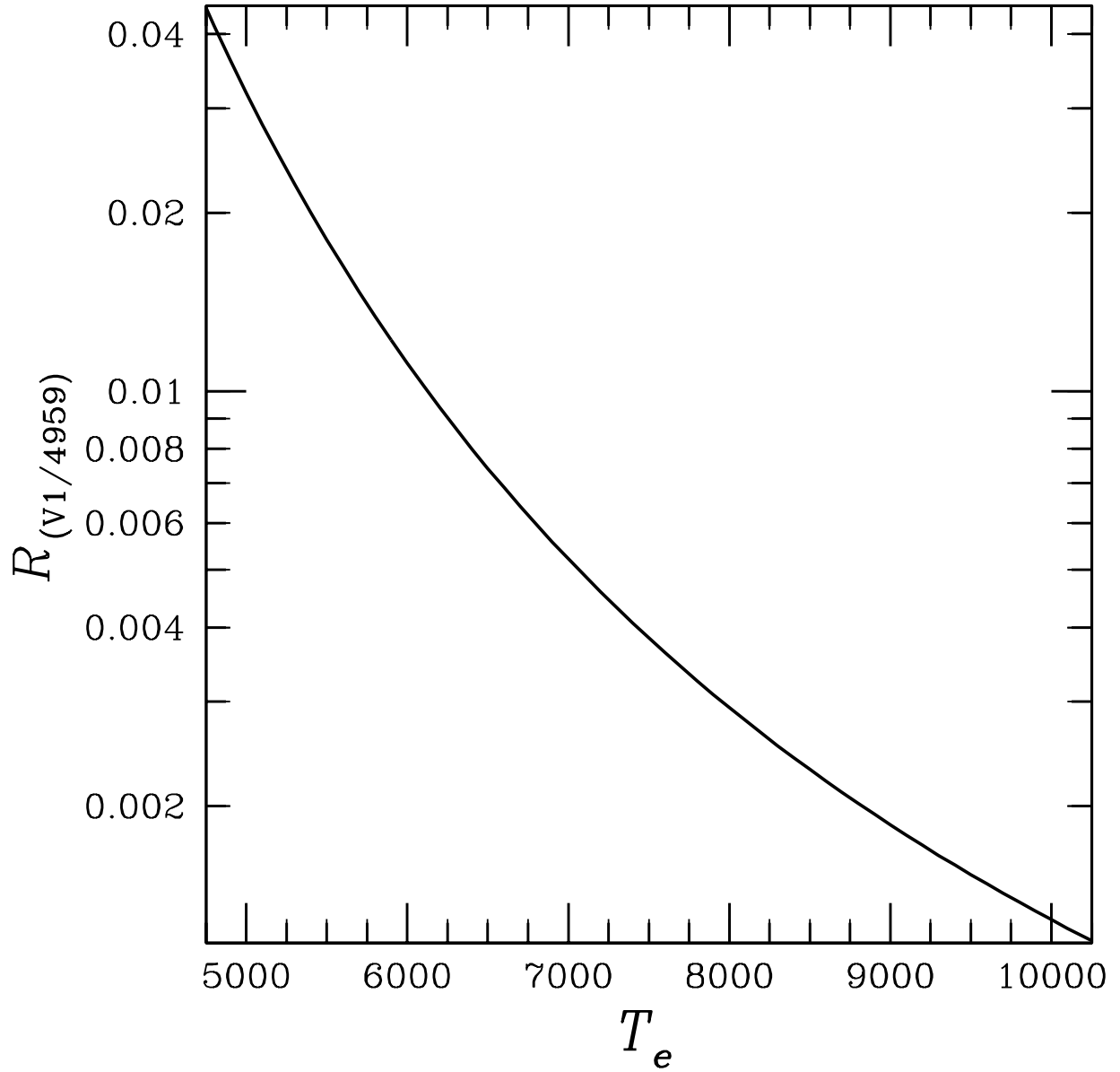


Fig. 1.— T versus $R_{(V1/4959)} = \varepsilon_{V1}/\varepsilon_{4959}$ derived from equation 6. For all the objects in the UVES sample $T_e(V1/4959)$ is smaller than $T_e(4363/4959)$, showing the presence of temperature inhomogeneities.

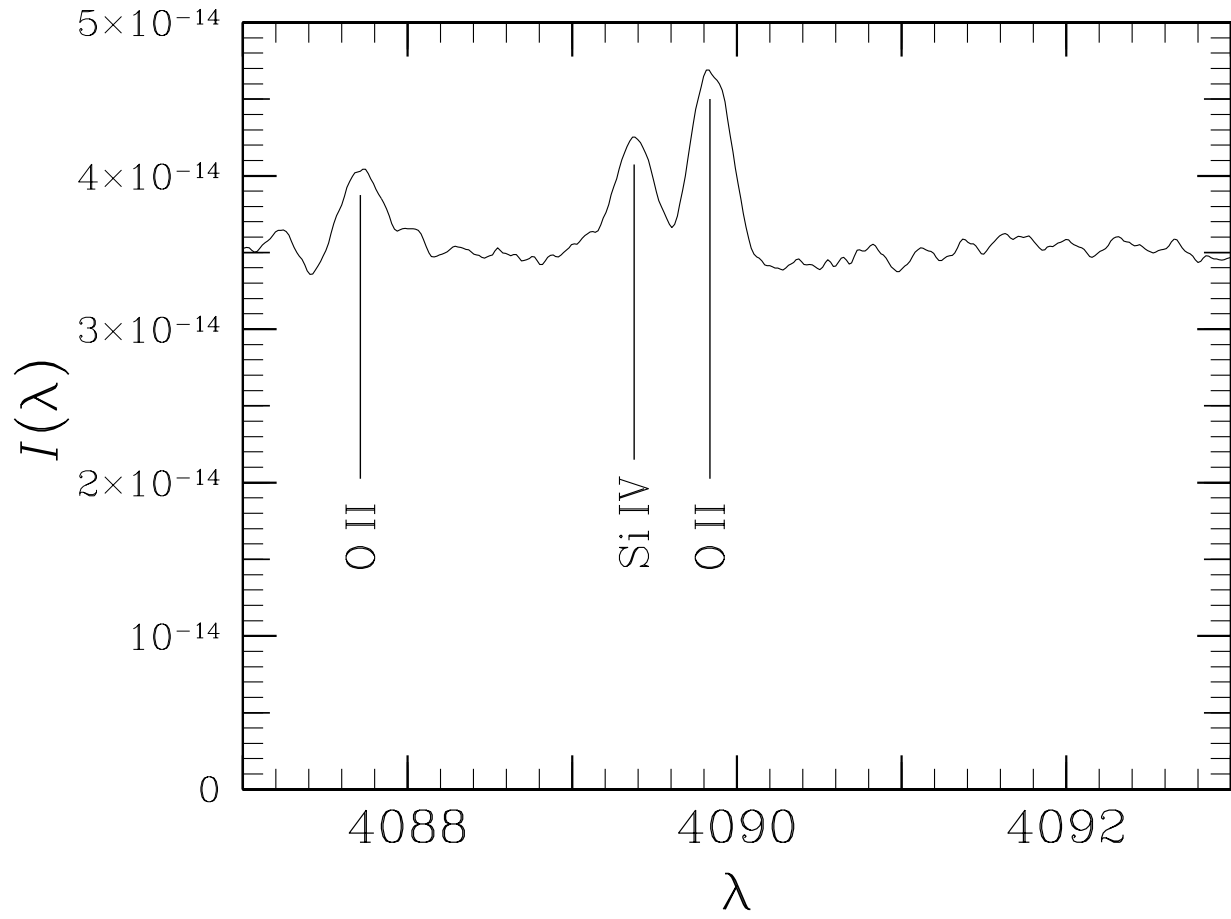


Fig. 2.— $I(\lambda)$ versus λ . Section of the UVES spectrum of the Orion nebula by Esteban et al. (2004) showing the presence of the Si IV $\lambda 4088.86$ line in emission.

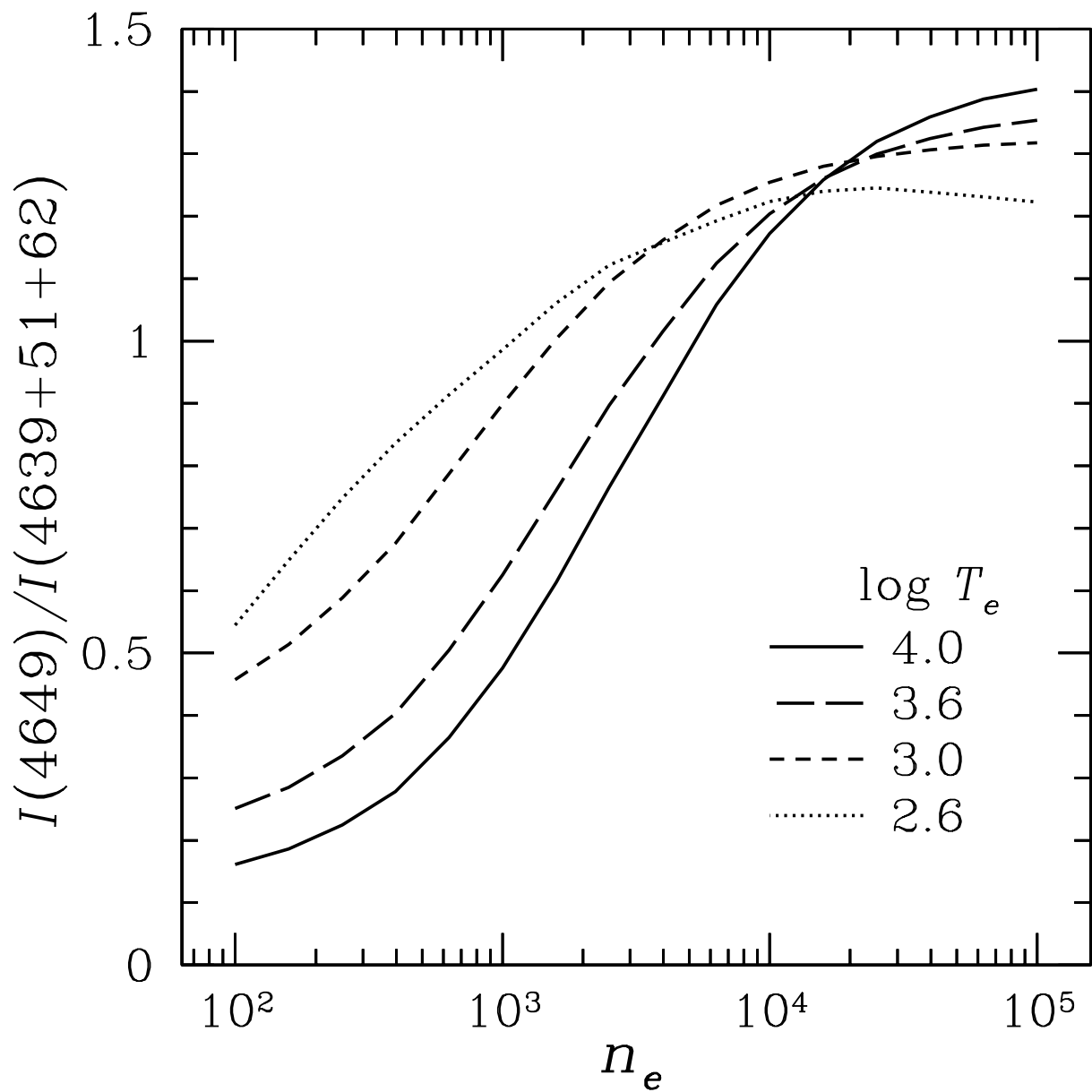


Fig. 3.— $I(4649)/I(4639 + 4651 + 4662)$ versus $n_e(\text{O II})$. Intensity density diagram of O II for different temperatures derived from the unpublished computations by Storey (Bastin & Storey 2006; Liu 2012; Fang & Liu 2013).

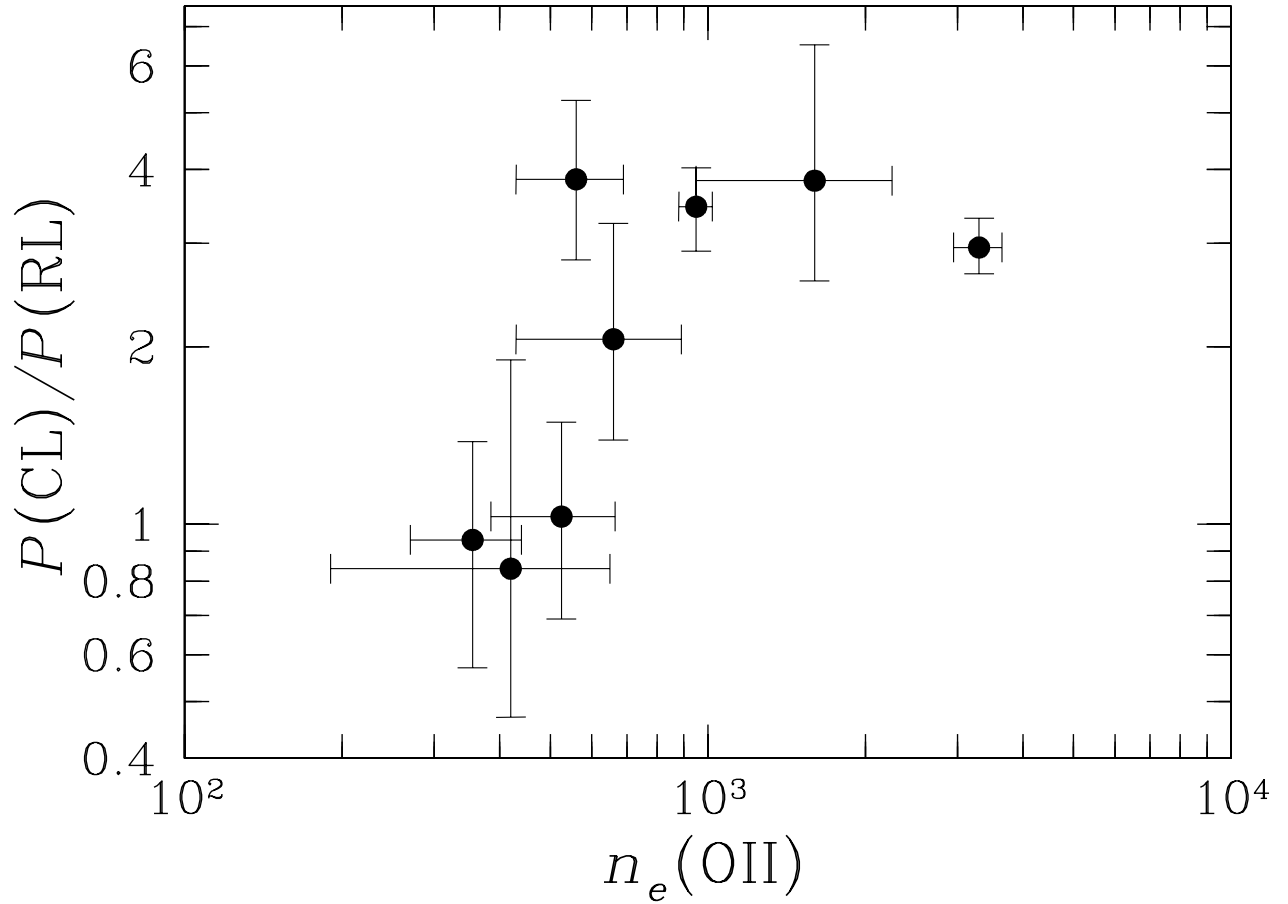


Fig. 4.— $P(\text{CL})/P(\text{RL})$ versus $n_e(\text{O II})$. Ratio of pressures derived from collisional to recombination lines as a function of the density obtained from the O II recombination lines. The data corresponds to the H II regions of the UVES set.